Performance of the SOAR adaptive module with UV Rayleigh guide star

Andrei Tokovinin, Roberto Tighe, Patricio Schurter, Rolando Cantarutti, Nicole van der Bliek, Manuel Martinez, Eduardo Mondaca, Steven Heathcote

Cerro Tololo Inter-American Observatory, Casilla 603, La Serena, Chile

ABSTRACT

The adaptive module of the 4-m SOAR telescope (SAM) has been tested on the sky by closing the loop on natural stars. Then it was re-configured for operation with low-altitude Rayleigh laser guide star in early 2011. We describe the performance of the SAM LGS system and various improvements made during one year of on-sky tests. With acceptably small LGS spots of $1.6''$ the AO loop is robust and achieves a resolution gain of almost two times in the I band, under suitable conditions. The best FWHM resolution so far is $0.25''$ over the $3'$ field of the CCD imager.

Keywords: Laser Guide Star, Adaptive Optics

1. INTRODUCTION

The idea of seeing improvement in a wide field by partial correction of low-altitude turbulence was proposed by Rigaut[4] in 2001 and rapidly gained popularity. Several Ground-Layer Adaptive Optics (GLAO) instruments are presently under development (e.g. ARGOS[2] or GRAAL[3]), while the GLAO mode at MMT is already used for science.[1] GLAO systems for extremely large telescopes are being proposed. The 4.1-m Southern Astrophysical Research Telescope (SOAR) is developing a GLAO system based on ultra-violet (UV) Rayleigh laser guide star (LGS). The SOAR Adaptive Module (SAM) is a facility instrument.[5, 8, 12, 13]

The SAM project was started at NOAO in 2002, 10 years ago. It passed the conceptual review (2003) and two preliminary design reviews (2005, 2007). The integration started in 2008. SAM was tested on the sky for a brief period in 2009,[13] then the integration and testing resumed. From November 2010 to January 2011 the AO system, guiders, and imager were commissioned using natural guide stars (NGS), while the laser components were still integrated and progressively deployed. The LGS loop was first closed in April 2011, demonstrating the resolution gain from GLAO. However, the instrument had (and still has) some technical issues that were addressed during the following year. As a result of gradual improvements, we achieved stable operation of the LGS AO loop and could take spectacular long-exposure images of selected astronomical objects.

The design of the SAM AO module has been described in Refs. 8, 12. A pair of off-axis parabolic mirrors re-images the focal plane onto science instruments with 1:1 scale while correcting turbulence with a 60-element bimorph deformable mirror (DM). The wavefront sensor (WFS) is of Shack-Hartmann type, with 10x10 sub-apertures and an e2v CCD-39 detector. In the LGS mode, tip-tilt is sensed with two natural guide stars (NGS) located outside the main field. The UV light is directed to the WFS, while visible light goes to science instruments. The CCD imager, SAMI, is part of SAM. It has 4096×4112 pixels with a pixel scale of 45 mas. Standard $BVRI$ and Hα filters are installed. Another SAM port can hold a small *visitor instrument*; presently it is the High-Resolution Camera[11] with a fast EM-CCD.

We present main parameters of the SAM LGS system in Sect. 2, focusing in Sect. 3 on the improvement of the LGS angular size which turned out to be critical for SAM operation. Section 4 details the performance of two tip-tilt loops, Sect. 5 describes the high-order AO loop operation. Examples of compensated images and some data on the delivered image quality are presented in Sect. 6. The paper closes with an outlook in Sect. 7.

E-mail: atokovinin, rtighe, pschurter, rcantarutti, nvdbliek, mmartinez, emondaca, sheathcote@ctio.noao.edu

2. THE UV LASER GUIDE STAR

The design of the SAM LGS system was presented in Ref. 13; it is recalled here briefly. The UV (355 nm) LGS is created by a pulsed frequency-tripled Nd:YAG laser (Q301-HD from JDSU). Its nominal 10 W power at 10 kHz pulse frequency has been verified in the laboratory, but the actual power at the telescope is about 7.5 W. The laser is mounted on the telescope truss and works under variable gravity direction. The container with the laser, 8x beam expander and auxiliary elements is stabilized in temperature at $+20°$C. The laser operated so far without any faults, as a turn-key device. Expanded parallel 8-mm beam is directed towards the Laser Launch Telescope (LLT) with one reflection from a flat mirror M4 which is remotely controlled in tip and tilt for beam alignment. The propagated beam has circular polarization.

The LLT (Fig. 1) is a reflective Dull-Kirkham afocal telescope with a 15-mm spherical secondary and a 250-mm elliptical primary mirror (optical de-magnification 28). The focal length of the primary (M1) is 420 mm. Its Astro-Sitall substrate is light-weighted to a mass of 1.2 kg. The mirror is mounted on three flexures which are attached to the Invar pads glued in the substrate. These flexures replace traditional mirror cell and allow pointing actuation.[13] Fast pointing corrections are made by a small flat mirror mounted on a tip-tilt piezo platform inside the LLT. This tip-tilt mirror with dielectric coating transmits visible light, so images of stars can be captured by a small camera behind this mirror to check LLT pointing and optical quality. The LLT is protected by a box-shaped enclosure opening at the top.
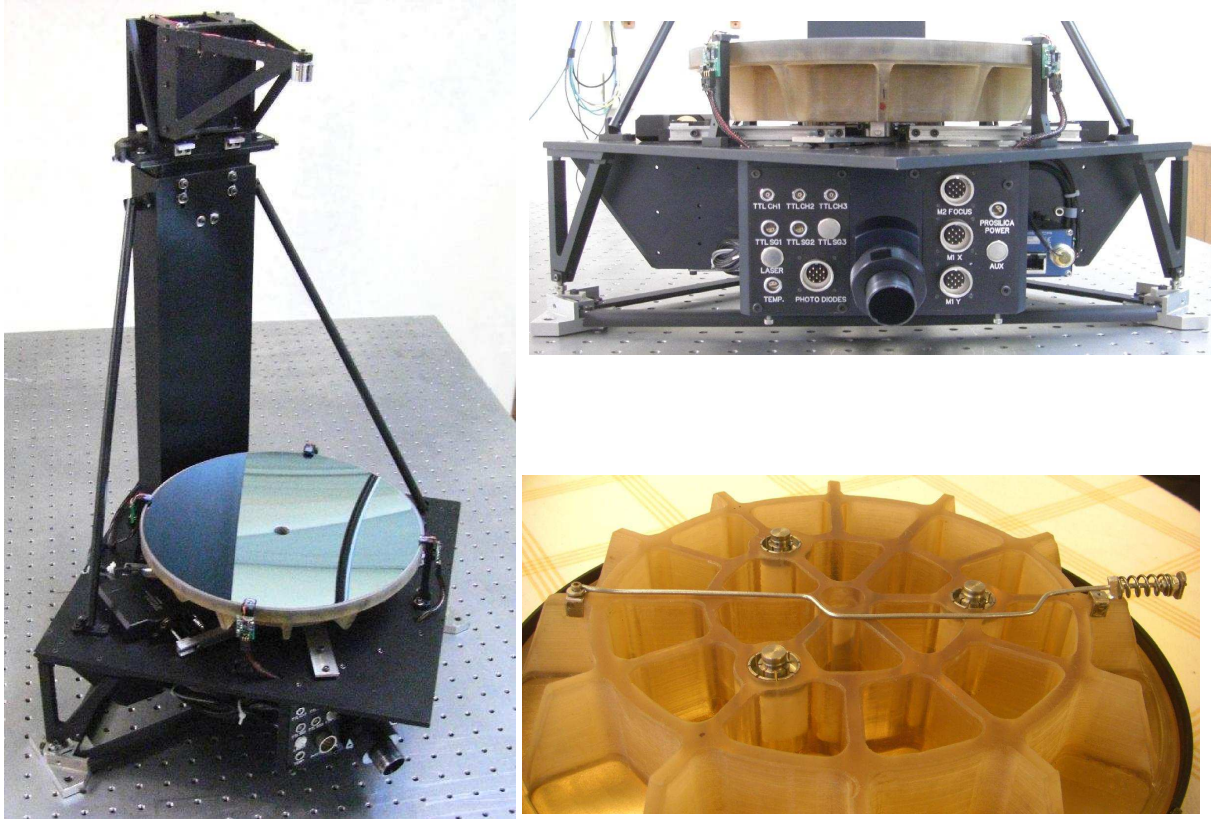

Figure 1. Laser Launch Telescope of SAM. Left: overall view without enclosure. Top-right: view from the connector panel. Lower-right: light-weighted primary mirror with three "flexible" Invar inserts and an adjustable spring to correct the astigmatism.

Figure 2 shows the footprint of the UV laser beam exiting the LLT. The beam is visualized by fluorescence of white paper, photographed by a normal camera. The size of the Gaussian beam was adjusted to a FWHM of 125 mm, close to its optimum value (a smaller beam is enlarged by diffraction, a larger beam loses energy outside
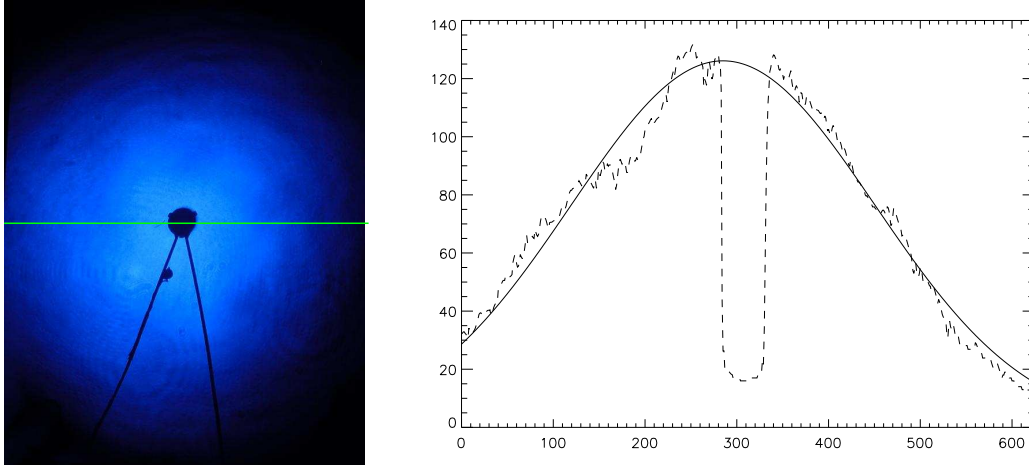
Figure 2. Left: image of the LGS beam at the LLT exit, with a shadow of its secondary mirror. Right: profile of the central cross-section with a fitted Gaussian, FWHM 125 mm.

working aperture). Four UV photo-diodes around M1 border allow us to center the beam remotely by actuating the fold mirror M4.

Back-scattered UV photons are collected by the SOAR telescope, pass through the SAM optics, and create the LGS image in its WFS. The Pockels-cell fast shutter inside the WFS transmits light only during a short time-gate pulse. The delay of the gate determines the distance z to the LGS (nominally $z = 7\,\mathrm{km}$), the gate duration sets the LGS axial size δz (typically $150\,\mathrm{m}$). The WFS has a pixel scale of $0.375''$ with 8x8 pixels per sub-aperture and 10x10 sub-apertures across the pupil. This fine scale and small $2.8''$ field size are not optimum for the LGS, and we consider replacing the lenslet array with one of shorter focal length.
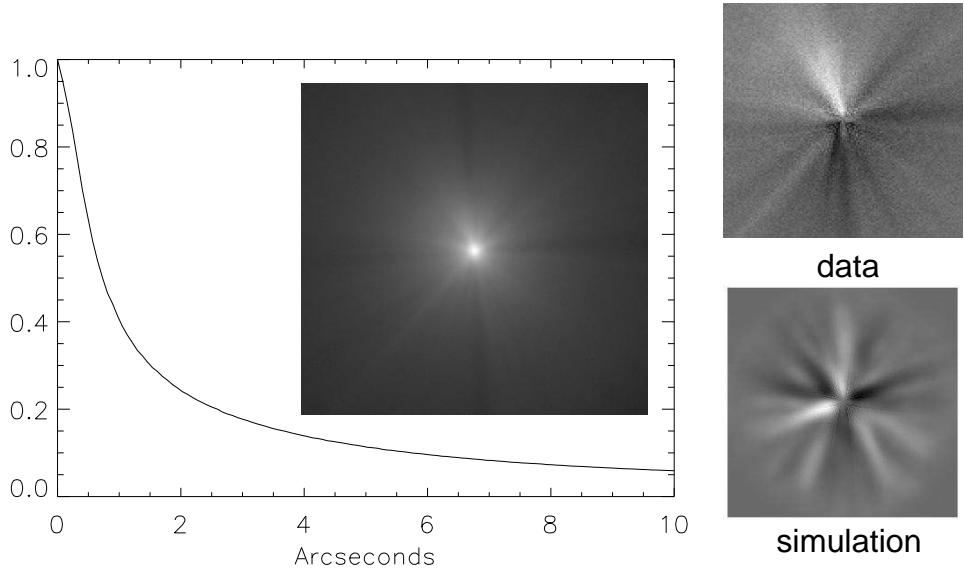

Figure 3. Radial profile of the un-gated LGS image in the WFS acquisition camera taken on December 7, 2011. The large insert shows the image itself. Radial "rays" are enhanced by subtracting the azimuthally-averaged profile (top right).

For acquisition of the LGS, its un-gated image can be captured by a small CCD (Prosilica GC 650) fed by a 45° mirror that slides in front of the WFS aperture (Fig. 3). The WFS is nominally focused at $7\,\mathrm{km}$. Even the un-gated LGS image is quite sharp. Geometric optics predicts its intensity profile inversely proportional to

the radius, $I(r) \propto 1/r$. Due to the finite size of the LGS and other broadening factors such as seeing and SOAR optics, the central intensity is not infinite. Modeling shows that the FWHM of un-gated LGS profile is 1.40 times larger than the FWHM of the LGS itself. Therefore, the LGS size can be measured on un-gated images.

When the LGS angular size is small as in Fig. 3 (intrinsic size $1''$), we see light and dark "rays" around it that move randomly. Those rays are produced by phase distortions which cause intensity modulation out of focus (un-gated image is a superposition of defocused images reminiscent of curvature sensing). Indeed, we simulated the "rays" by co-adding many images with positive and negative defocus produced by the same phase distortion at the pupil.

A typical return flux on a clear night is about 1000 photons per sub-aperture per loop cycle with a range gate of $1\,\mu$s ($\delta z = 150$ m). The flux can be twice higher at certain position angles of the instrument (we have not yet tuned the WFS polarizing optics optimally) and much lower when the LGS size is large.

3. SIZE OF THE LGS SPOTS

Despite first successful closed-loop operation in April 2011, the quality of the SAM LGS was disappointing. Quite often "fuzzy" spots filled the whole WFS field. Moreover, the spot size varied during the same night in a seemingly random way (Fig. 4). Fuzzy spots prevented AO loop operation and substantially reduced the return flux (photons were scattered outside the $2.8''$ WFS aperture).

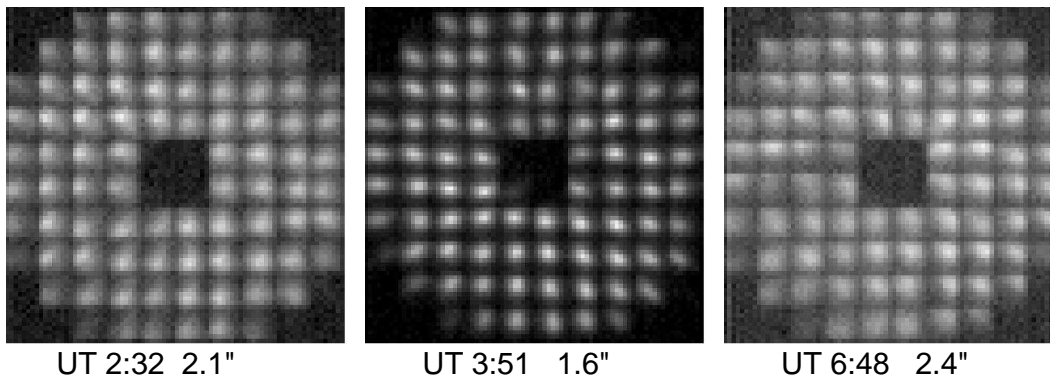| UT 2:32 2.1" | UT 3:51   1.6" | UT 6:48   2.4" |

Figure 4. LGS spots on January 10, 2012. The UT time and FWHM are indicated in the Figure.

Our first suspicion turned on the optics. The laser beam quality is very high ($M^2 = 1.04$ measured in the laboratory). The LLT optics was tested by the manufacturer (S. Potanin and his colleagues at the Sternberg Astronomical Institute in Moscow). It has ~ 90 nm rms low-order wavefront aberration (mostly astigmatism) and, in addition, circular zonal errors ("ripple") with a rms wavefront error of 21 nm. These data were confirmed independently during LLT integration. Extensive simulations convinced us that this optics should form a sub-arcsecond UV image under $1''$ seeing. The ripple throws about 13% of the UV light into a wide halo.

Images of stars with the LLT have shown that a notable triangular distortion appeared in May and June 2011, something that was not seen in February or in the lab. The reason was eventually traced to the thermal effect of the Invar inserts in the LLT primary mirror. The CTEs of Invar and Astro-Sitall are close enough, but the thin layer of the epoxy glue could have caused this problem. The inserts were replaced by a "flexible" design which solved the problem (small size of the LLT allows its cold optical test in the standard fridge).

The quest for a reduced LGS size has led us to other discoveries and improvements, such as re-alignment of the beam expander, replacement of the burned plastic spacer around M2, and minor mechanical modifications of the LLT. Even the astigmatism of the M1 was removed by an adjustable spring that created opposite deformation. The LLT optics was tested in auto-collimation after its re-installation at SOAR in November 2011, and later. Encouragingly good spots were obtained sometimes (Fig. 3), with the smallest FWHM of $1.3''$. Yet the spots became fuzzy on and again (Fig. 4).

Temporal variability of the LGS size convinced us that the main cause of its broadening is a local turbulence near the LLT. Two electronic boxes mounted just below the LLT and a small sky camera near it create warm air
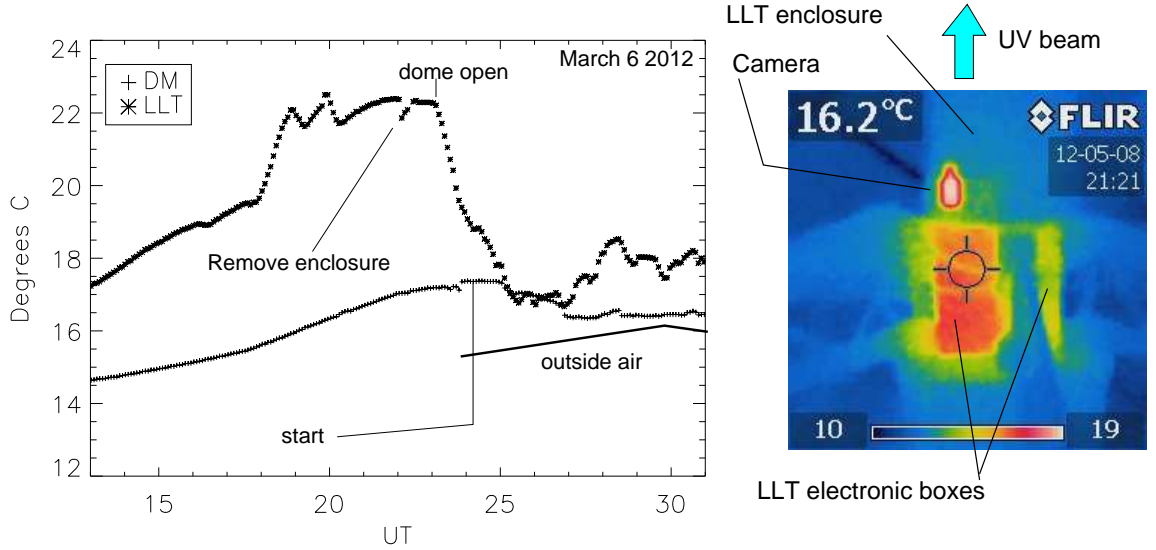
Figure 5. LLT temperature on March 6/7 2012. For comparison, the temperature of the SAM deformable mirror (DM) is plotted. The LLT was heated during the day (it is in the upper part of the dome), but cooled down rapidly when the dome was opened in the evening. During first half of the night the LLT pointed into the wind and had same temperature as the DM, but in the morning the telescope pointed to the South and the LLT became warmer by $\sim 2°$. On that night the LLT worked without enclosure. Thermal image on the right shows heat sources near the LLT.

that can get in the light path, depending on the orientation with respect to the wind (Fig. 5). Indeed, we noted that the LGS spots were good and the LLT temperature low when looking into the wind (to the North), while targets in the South had worse spots. Better spots were obtained when the LLT enclosure was removed, as on March 6/7 2012, and on windy nights (May 8, 2012). We plan to address the issue by re-locating and modifying the LLT electronics.

4. TWO TIP-TILT LOOPS

Tip-tilt (tt) errors are compensated by the fast tertiary mirror of the SOAR telescope. It is driven by average signal from two tt guide stars chosen within the square SAM technical field of $5' \times 5'$, preferably avoiding the central $3' \times 3'$ science field. The guide probes are located in the telescope focal plane, up-stream from the DM (in the LGS mode the DM is not supposed to create variable tilts). Each guide probe is an array of 2x2 micro-lenses forming a quad-cell position sensor. The quadrants are fiber-coupled to avalanche photo-diodes.

The guiding was tested when SAM worked in the NGS mode, enabling independent measurement of the residual tilt with the WFS. We established the response factor R – relation between dimensionless quad-cell signal and image displacement x, $e_x = Rx$. Typically $R \approx 1.35 \, \text{arcsec}^{-1}$, in agreement with the expected image size. The response is measured in three different ways: by comparing the residual rms tilt measured by the WFS with the residual rms of e_x, by guiding with one probe and scanning the other probe, and by recording reaction of the probes to a small circular wobble of the SOAR tt mirror with known amplitude.

The total counting rate F in each probe is related to the stellar magnitude V as

$$F[\text{kel/s}] = 10^{0.4(V_0 - V)}, \tag{1}$$

where V_0 is the zero point (magnitude of a star giving 1 kel/s). The average empirical zero points are 19.9 and 19.7 for the two probes of SAM, matching their estimates. However, the scatter around this average relation is very large, signaling that stellar magnitude in the USNO catalog used for the calibration are inaccurate.

The tt servo loop compensates frequencies below $\sim 4 \, \text{Hz}$. Median residual tt error measured by the NGS WFS (while guiding with the probes) is slightly better than $0.1''$. This is confirmed by the analysis of fast image

sequences recorded with HRCam. Interestingly, when the tilt error is small, about 50 mas rms, the correlation of residuals between the probes is always negative, meaning that tilt anisoplanatism is the main contributor (the average tilt is compensated, so individual residuals are of opposite signs). On the other hand, records with the largest errors (up to 0.18″) always show a positive correlation between the probes, meaning that the servo system was unable to track strong or fast pointing errors of SOAR.

Motion of the SOAR tt mirror also affects the LGS position. Therefore, another tt loop has to keep the LGS spots centered in the WFS, compensating this perturbation, the up-link tilt in the LLT, and eventual mechanical drifts. The average slopes measured by the WFS are transformed into control signals that drive the tt piezo-platform of the LLT. This *LLT loop* is closed after locking on the guide stars, but before closing the main AO loop. This loop works up to $\sim 7\,$Hz and leaves rms residuals from 0.07″ to 0.12″. This is small enough in comparison with the WFS field, but still a major component of the residual slope variance. Figure 6 illustrates the operation of the LLT loop: while the piezo platform tracks large low-frequency tilt errors of SOAR, the residual global tilt measured by the WFS is small and has a normal distribution.
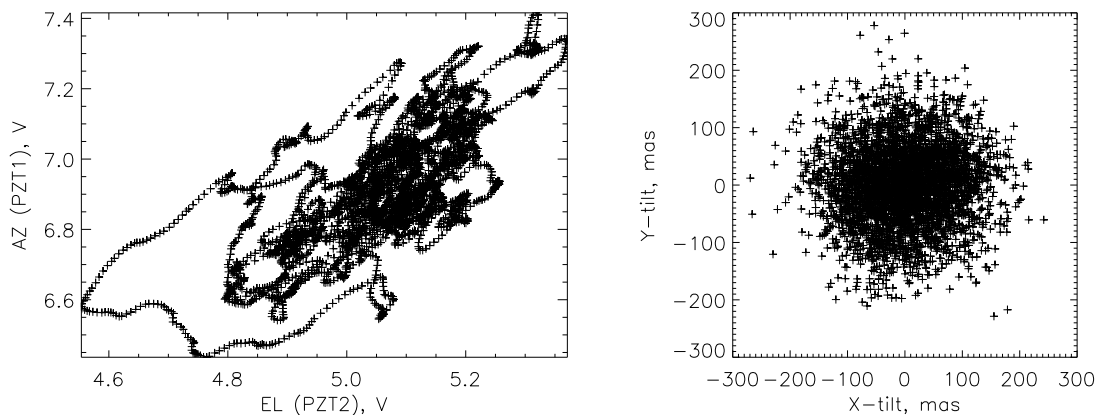

Figure 6. Left: evolution of voltage on the LLT tip-tilt piezo platform for the loop data of UT 7:30 on May 9, 2012. Right: evolution of residual LGS tilt in X and Y for the same data.

5. PERFORMANCE OF THE HIGH-ORDER AO LOOP

The high-order loop compensates turbulence by keeping spot centroids at zero. The loop frequency is 233 Hz (4.3 ms per cycle). SAM uses correlation centroid calculation,[6] standard SVD reconstructor, and integral controller with a gain of 0.25 and a leak coefficient of 0.99. The compensation quality is quantified by the rms slope residuals or, equivalently, by the residual variance of Zernike modes.

The noise of centroids is readily estimated from the difference between two successive loop cycles, dominated by the measurement errors rather than by the lag errors. We tested various centroid algorithms on the recorded sequences of real WFS images and found that for SAM the standard center-of-gravity (CoG) gives the lowest noise. This is natural because the LGS spots occupy nearly the whole WFS field. Correlation with a wide template (20 pixels FWHM) is essentially equivalent to the simple CoG. With a typical LGS spot FWHM of 1.6″, 10^3 photons per loop, and readout noise of 4.7 el, the centroid noise is 35 mas, in perfect agreement with its theoretical estimates.[6] We used a wrong (too small) template in the first LGS engineering runs.

Ground-layer turbulence is compensated by SAM only partially because of the fitting error (a much higher order is needed for a good correction in the visible), noise, lag, tilt, and other AO errors. The net result[10] is that the *residual structure function $E(r)$* is roughly proportional to the distance r, with a typical rms error of $\sqrt{E(1m)} = 0.4\,\mu$m. The corresponding PSF is well represented by a Moffat profile with $\beta = 1.5$ and its FWHM ϵ scales as $\epsilon = 0.5″\sqrt{E(1m)}/\lambda$ with wavelength λ in microns.[14] This has been verified when SAM worked with the NGS and compensated all turbulence in the light path on-axis.
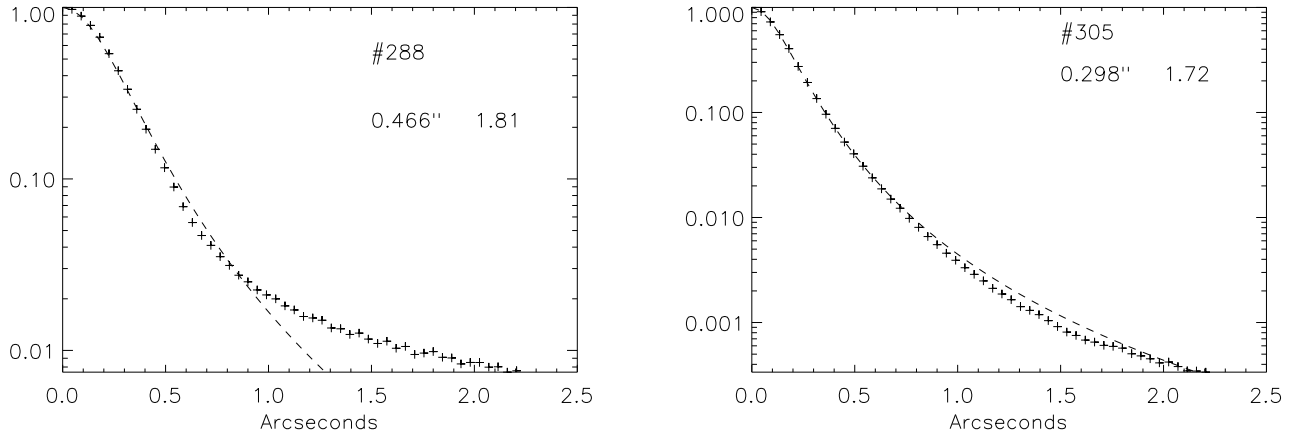
Figure 7. Radial profiles of the PSFs (pluses) and fitted Moffat models (dashed lines) of stars around the Boomerang nebula observed with SAM on March 6/7, 2012 (left – V filter, right – I filter). The FWHM and β are indicated on the plots.

In the case of LGS, the PSF is a convolution of residual blur from the partially compensated ground layer with seeing from high-altitude uncompensated turbulence. The relative contribution of those factors is variable, depending on the turbulence profile. The resulting PSF is fitted by a Moffat profile with parameter β from 1.5 to 2.5 (Fig. 7).
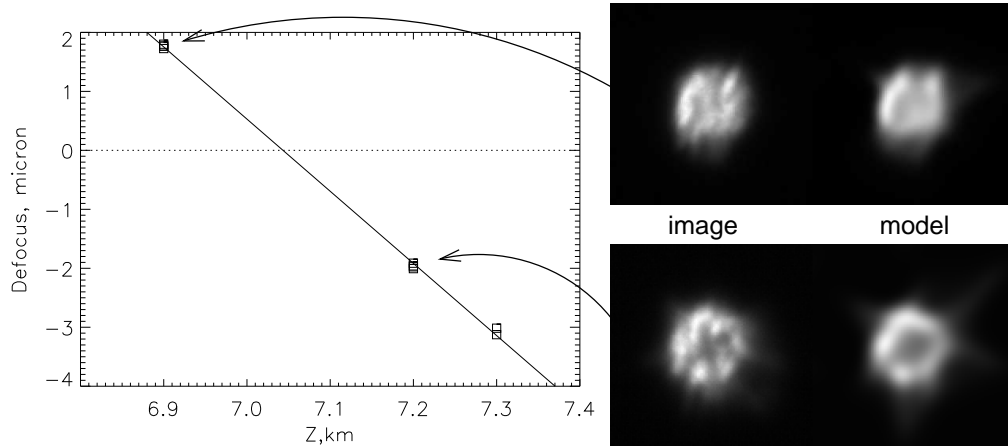

Figure 8. Focusing in the LGS mode. Long-exposure images in closed loop with intentionally de-tunes LGS range z are modeled by the *donut* algorithm.[9] This gives accurate estimates of defocus and establishes the optimum LGS range of 7.04 km.

The residual focus in the science instrument depends on the LGS range z, and on internal settings of SAM opto-mechanics. Focusing is thus non-trivial. We successfully tried a method where the range z is intentionally de-tuned to both sides of the expected focus and images in closed-loop are taken. If the expected focus is correct, the PSF width on both sides will be the same, otherwise the focus is found by linear interpolation. The procedure worked very well on May 8, 2012; for four targets we obtained the same optimum range. Defocused closed-loop images were processed off-line by fitting Zernike coefficients (*donut* models[9]). This allows us to evaluate low-order non-common-path errors as well. We found that the residual defocus coefficient a_4 vs. z falls on a straight line with a slope of $-12.24\,\mu m/km$ (Fig. 8), exactly as calculated. Other aberrations are small and vary randomly, except possibly some coma.

Once the optimum LGS range is found, focusing in open loop is easy. We simply adjust the telescope focus to get a near-zero a_4 by looking at its real-time display. Note that the DM in open loop does not maintain "flat" surface because of its flexure (SAM rotates to compensate parallactic angle), temperature, and creep. The flexure is well corrected by a model (terms proportional to sine/cosine of the rotator angle are added to the electrode voltages). Other effects are taken care of by frequent re-calibration of the flat DM on the internal UV source inside SAM. In November 2011, one of the HV amplifiers failed and the DM electrode #48 stayed at -400 V for a week. Since then, this electrode requires a positive voltage (60% of the dynamic range) to keep the DM flat. The DM thus suffered a permanent damage.

Quite often the SAM AO loop was unstable. It would diverge either immediately after closure or later. In this case the spots on one side of the telescope pupil disappear because the DM "wraps" too much and moves the light outside the WFS aperture. The "wraps" become systematic when the LGS spots are fuzzy and the return flux is low. They can either self-correct or lead to a DM saturation that requires operator intervention. "Wraps" result from a combination of several factors: large LGS spot size, small WFS field, and interaction between the AO and LLT loops. Recently we modified the control algorithm to prevent subtraction of the average tilt from sub-apertures without signal. The loop worked stably in the last engineering run (May 8 2012). Further work is needed to reach a robust AO loop operation.
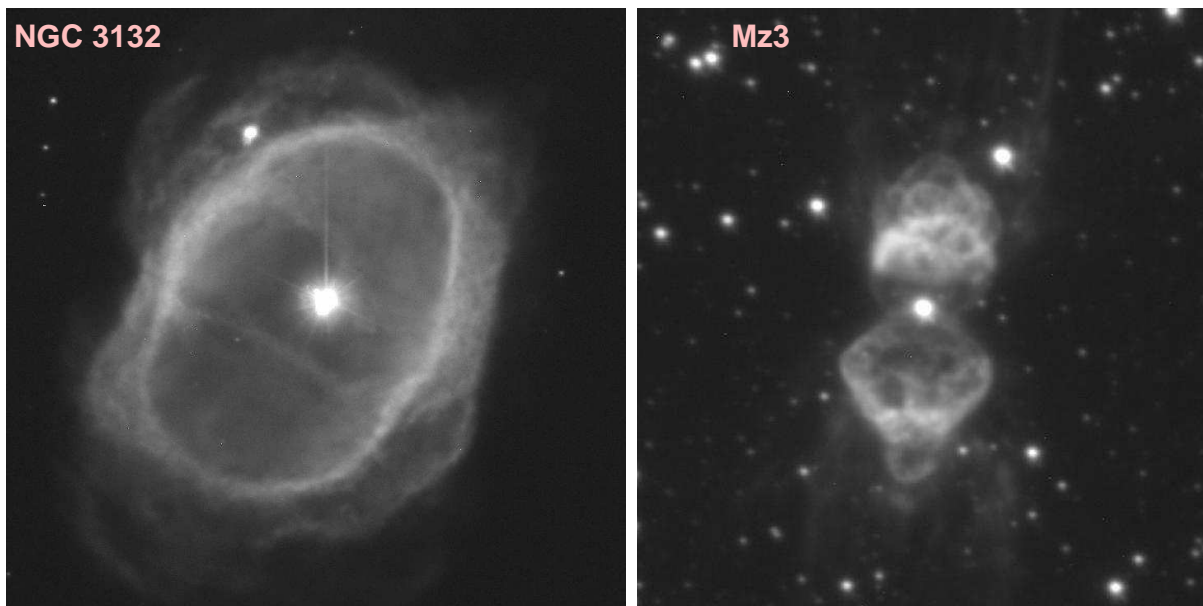
6. DELIVERED IMAGE QUALITY

Figure 9. Images of planetary nebulae with SAM. Left: NGC 3132 (R, 60s, FWHM $0.24''$) on March 6/7, 2012. Right: Mz3 (R, 180s, FWHM $0.53''$) on May 8/9, 2012.

During two engineering runs in March and May 2012 the SAM AO system worked stably because the LGS spot size was small, around $1.6''$ on average. Atmospheric conditions on those two nights seem to be favorable for GLAO, although this is only a guess (the site monitor at Cerro Pachón was out of service). Without turbulence profiles, we can't make a fair comparison between the delivered SAM performance and its expectation.[7] The gain in resolution achieved in closed loop was however substantial. Figure 9 shows images of emission nebulae taken with SAM. Presumably, they are the best ground-based images of those objects which, however, can't compete with the Hubble Space Telescope. Figure 10 gives another illustration of the SAM gain.

It is premature to give statistics of SAM performance: more data are needed. Histograms of FWHM resolution in open and closed loop for one night are given in Fig. 11. Such histograms were made for all filters and show how the ground-layer correction improves at longer wavelengths. On the night of March 6/7 SAM provided substantial gain even in the blue B filter.
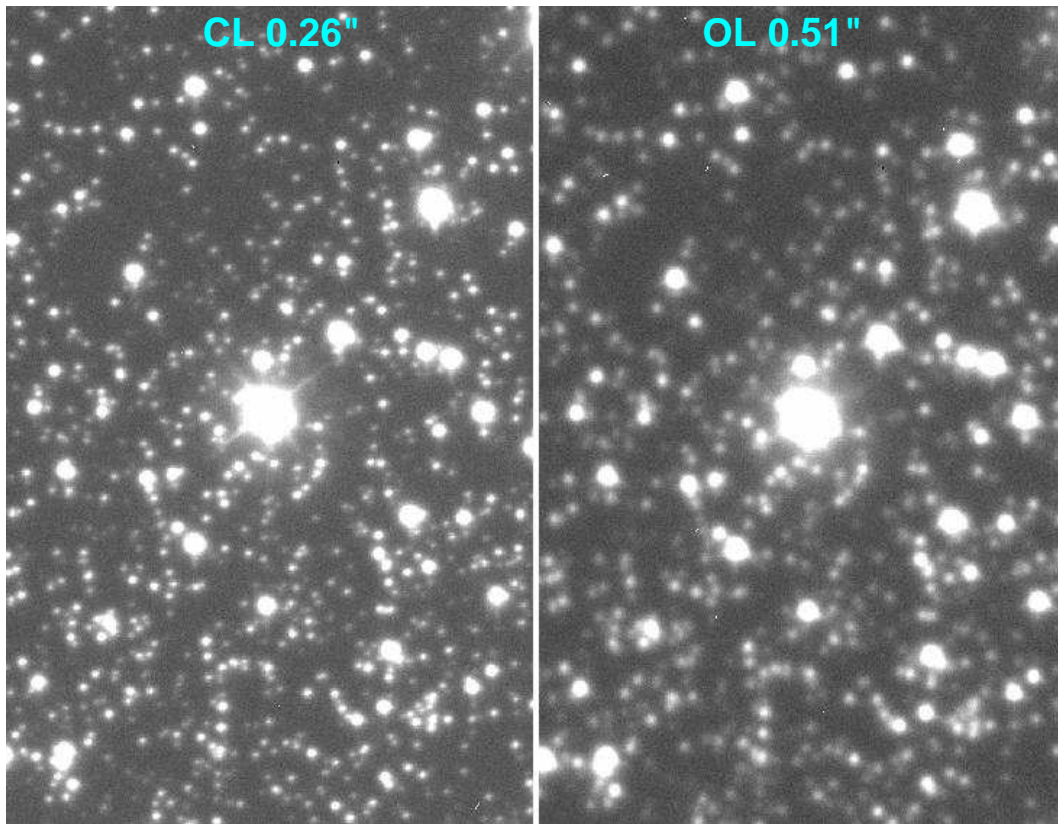
Figure 10. Pair of 120-s exposures of globular cluster NGC 6496 in closed (left) and open (right) loop in the *I* band on May 8/9, 2012. Matching fragments near the center are shown with FWHM of $0.26''$ and $0.51''$, respectively.
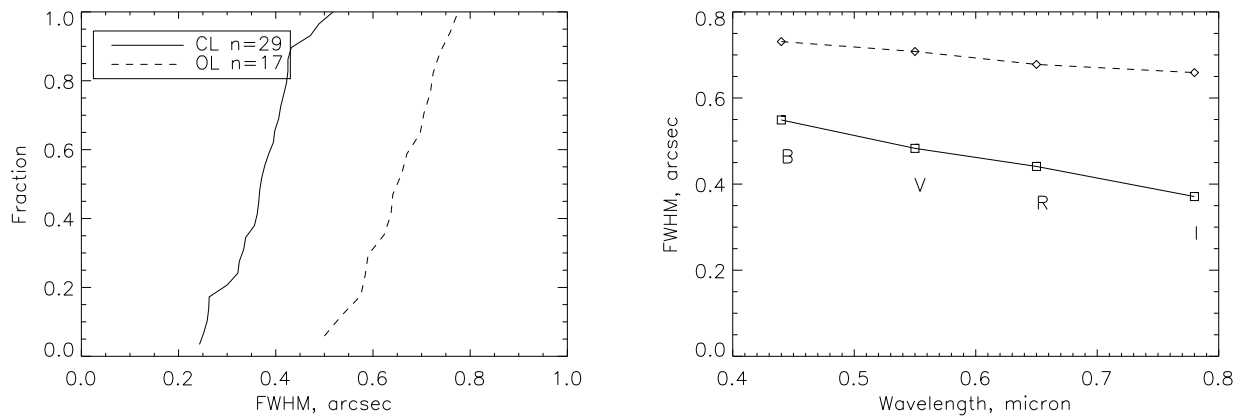

Figure 11. Left: cumulative histograms of FWHM resolution in open (dashed lines) and closed (full lines) loop for all SAM data of March 6/7, 2012, in the *I* filter. Right: median FWHM resolution vs. wavelength in open (dashed line) and closed (full line) loop for the same night.

The resolution of SAM can be further improved. We found a gradient of FWHM in the latest SAMI images that can be indicative of a detector tilt (to be investigated). The new focusing procedure and elimination of non-common-path errors need more work, as well as the AO loop optimization.

7. CONCLUSIONS AND OUTLOOK

The SAM LGS system deployed in 2011 required patient work before it could be operated stably and demonstrated its potential. We were fortunate to commission the AO module with NGS, allowing us to focus later on the LGS system almost exclusively.

Various hardware and software issues still remain to be fixed before SAM approaches the state of a facility instrument. We need to eliminate heat sources around the LLT that degrade the laser spot size and to tune the polarization in the SAM WFS. Replacing the lenslet array in the WFS will improve its performance and the loop robustness. Acquisition of guide stars is cumbersome because the probes have a small $1.5''$ capture field while our software tools and used catalogs are not good enough to point blindly with such accuracy. We contemplate equipping each probe with a small acquisition camera (webcam).

Our accumulated experience indicates that SAM operation can be made easy. Once the planned tools and fixes are implemented, the acquisition of guide stars and LGS and closing the loops will become a quick routine action. The complexity of laser-assisted AO will be hidden from the SAM operator, converting the instrument into a friendly seeing-enhancement tool for astronomers.

REFERENCES

[1] Bendek, E. A., Hart, M., Powell, K. B., Vaitheeswaran, V., McCarthy, D. & Kulesa, C. "Latest GLAO results and advancements in laser tomography implementation at the 6.5m MMT telescope," Proc. SPIE, 8149, paper 6 (2011).

[2] Hart, M., Rabien, S., Busoni, L. et al. "Status report on the Large Binocular Telescope's ARGOS ground-layer AO system," Proc. SPIE, 8149, paper 18 (2011).

[3] Paufique, J., Bruton, A., Glindemann, A. et al. "GRAAL: a seeing enhancer for the NIR wide-field imager Hawk-I," Proc. SPIE, 7736, paper 57 (2010).

[4] Rigaut, F.. "Ground Conjugate Wide Field Adaptive Optics for the ELTs," in: Beyond Conventional Adaptive Optics, eds. E. Vernet, R. Ragazzoni, S. Esposito, N. Hubin, ESO Conf. Workshop Proc. 58, ESO, Garching bei Munchen, p. 11 (2002).

[5] Tokovinin, A., Gregory, B., Schwarz, H., "Visible-light AO system for the 4.2-m SOAR telescope," Proc. SPIE 4839, 673-680 (2003).

[6] Thomas, S., Fusco, T., Tokovinin, A., Nicolle, M., Michau, V., Rousset, G. "Comparison of centroid computation algorithms in a Shack-Hartmann sensor," MNRAS, 371, 323 (2006).

[7] Tokovinin, A., "Seeing improvement with ground-layer adaptive optics," PASP, 116, 941 (2004).

[8] Tokovinin, A., Thomas, S., Gregory, B., van der Bliek, N., Schurter, P., Cantarutti, R., Mondaca, E., "Design of ground-layer turbulence compensation with a Rayleigh beacon," Proc. SPIE, 5490, 870-878 (2004).

[9] Tokovinin, A., Heathcote, S. "Donut: measuring optical aberrations from a single extra-focal image," PASP, 118, 1165 (2006).

[10] Tokovinin, A., "Performance and error budget of a GLAO system," Proc. SPIE 7015, paper 77 (2008).

[11] Tokovinin, A., Cantarutti, R., "First speckle-interferometry at SOAR telescope with electron multiplictaion CCD," PASP, 120, 170-177 (2008).

[12] Tokovinin, A., Tighe, R., Schurter, P., Cantarutti, R., van der Bliek, N., Martinez, M. Mondaca, E., Montane, A., "SAM - a facility GLAO instrument," Proc. SPIE, 7015, paper 157 (2008).

[13] Tokovinin, A., Tighe, R., Schurter, P., Cantarutti, R., van der Bliek, N., Martinez, M. Mondaca, E., Montane, A., Naudy Cortes W. " SAM sees the light," Proc. SPIE, 7736, paper 132 (2010).

[14] Tokovinin, A., "GLAO4ELT: a trade study and SAM experience," Conference AO4ELT2, Victoria, September 25-30 (2011).